Progress in Biophysics and Molecular Biology 100 (2009) 40–46

Contents lists available at ScienceDirect

Progress in Biophysics and Molecular Biology

journal homepage: www.elsevier.com/locate/pbiomolbio

Review

Spatiotemporal modelling of CheY complexes in *Escherichia coli* chemotaxis

M.J. Tindall [a,b,*], S.L. Porter [c], G.H. Wadhams [c], P.K. Maini [b,c], J.P. Armitage [c]

[a] Institute for Cardiovascular and Metabolic Research and School of Biological Sciences and Department of Mathematics, University of Reading, Whiteknights, Reading, Berkshire RG6 6AP, UK
[b] Centre for Mathematical Biology, Mathematical Institute, University of Oxford, 24-29 St Giles', Oxford OX1 3LB, UK
[c] Oxford Centre for Integrative Systems Biology, Department of Biochemistry, University of Oxford, South Parks Road, Oxford OX1 3QU, UK

ARTICLE INFO

Article history:
Available online 18 June 2009

Keywords:
Bacterial chemotaxis
Phosphotransfer
Complex formation
Spatiotemporal mathematical modelling
Signal transduction

ABSTRACT

The chemotaxis pathway of *Escherichia coli* is one of the best studied and modelled biological signalling pathways. Here we extend existing modelling approaches by explicitly including a description of the formation and subcellular localization of intermediary complexes in the phosphotransfer pathway. The inclusion of these complexes shows that only about 60% of the total output response regulator (CheY) is uncomplexed at any moment and hence free to interact with its target, the flagellar motor. A clear strength of this model is its ability to predict the experimentally observable subcellular localization of CheY throughout a chemotactic response. We have found good agreement between the model output and experimentally determined CheY localization patterns.

Contents

1. Introduction 40
2. Modelling complex formation in the phosphotransfer cascade 41
3. Results and discussion 43
   3.1. Spatial distribution of CheY in wild-type cells 43
   3.2. Dynamic variation of CheY containing complexes in a wild-type cell 44
   3.3. Effect of CheZ expression levels on the spatial distribution of CheY 44
   3.4. Analysis of CheY complex formation 45
4. Conclusions 45
   Acknowledgements 46
   References 46

1. Introduction

Chemotaxis is the process by which bacteria detect the concentration of chemicals in their environment and bias their movement so that they accumulate in regions that are optimal for growth. This pathway has been most extensively studied in the Gram-negative rod-shaped bacterium, *Escherichia coli* (Wadhams and Armitage, 2004). Importantly, the localization (Maddock and Shapiro, 1993; Sourjik and Berg, 2000), copy number (Li and Hazelbauer, 2004) and reaction kinetics (www.pdn.cam.ac.uk/groups/comp-cell/Rates.html) of most of the components of this pathway have been experimentally determined.

For a review of bacterial chemotaxis see Wadhams and Armitage (2004). Briefly, chemicals, either attractants or repellents, are sensed by transmembrane chemoreceptor proteins (MCPs), which are localized along with CheW and CheA in clusters at the poles of the cell (Maddock and Shapiro, 1993; Sourjik and Berg, 2000). Ligand binding to these chemoreceptor clusters modulates the autophosphorylation rate of the associated histidine protein kinase, CheA. A decrease in attractant concentration or an increase in repellent concentration causes the chemoreceptors to activate CheA autophosphorylation. The phosphoryl group is then transferred from CheA to the response regulator, CheY. Once phosphorylated,

* Corresponding author at: School of Biological Sciences & Department of Mathematics, University of Reading, Whiteknights, Reading, Berkshire RG6 6AP, UK. Tel.: +44 118 378 7048; fax: +44 118 378 6537.
E-mail address: m.tindall@reading.ac.uk (M.J. Tindall).

0079-6107/$ – see front matter © 2009 Elsevier Ltd. All rights reserved.
doi:10.1016/j.pbiomolbio.2009.06.005

CheY$_P$ is released by the polar cluster and diffuses through the cytoplasm to interact with the FliM component of the flagellar motor (Fig. 1). CheY$_P$ binding to FliM induces a switch in the direction of flagellar rotation from counter-clockwise to clockwise, which leads to a change in swimming direction. Dephosphorylation of CheY$_P$ is required for signal termination. This hydrolysis reaction occurs spontaneously but is accelerated $\sim$ 100-fold by binding the phosphatase, CheZ, which is localized along with CheA to the polar clusters. A second response regulator, CheB, competes with CheY for phosphorylation by CheA. CheB is a component of the adaptation system, which in conjunction with CheR resets the signalling state of the chemoreceptors so that they return the activity of the CheAs to the pre-stimulus level despite the presence of a persistent stimulus. The response and adaptation pathways occur on different timescales, with cells responding to stimuli in $\sim$0.2 s and adapting over the course of several seconds.

The remarkable sensitivity and gain of the chemotaxis pathway in *E. coli* makes this pathway a particularly intriguing biological system to study. This manuscript builds upon the pioneering work of Dennis Bray and co-workers, who utilized experimental knowledge to inform computational models. In particular, they demonstrated the inability of the phosphotransfer network to describe gain within this pathway and proposed that interactions within the receptor clusters could account for the observed gain (Bray et al., 1998). In this manuscript we present a spatiotemporal model of the complexes formed during phosphotransfer using the theory of nonlinear reaction diffusion equations. The model explicitly describes the dynamic variation of CheY localization seen experimentally during a chemotactic response by including the presence of CheY containing protein-complexes. Our work demonstrates the importance of complex formation by showing that only 60% of the total CheY is uncomplexed.

2. Modelling complex formation in the phosphotransfer cascade

Consider a single *E. coli* cell in which CheA and CheZ are constrained to the polar clusters (regions Ω_2 and Ω_3 as shown in Fig. 2)

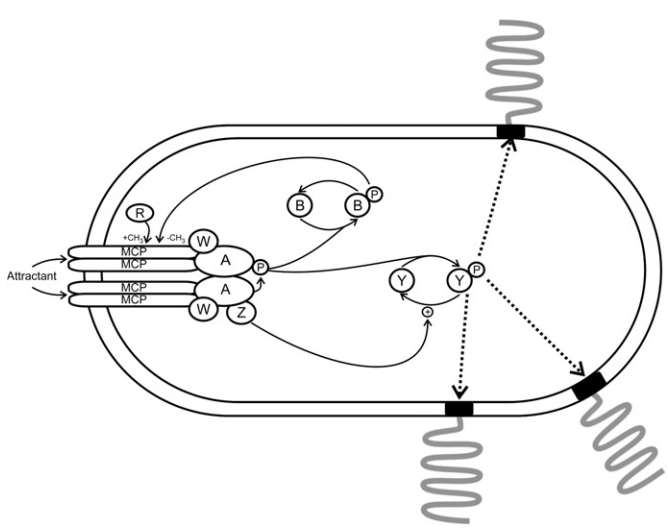

Fig. 1. The chemotaxis pathway of *E. coli*. Attractants are detected by transmembrane chemoreceptors (MCPs). These proteins form a complex at the cell poles with CheA (A), CheW (W) and CheZ (Z). The MCPs control the rate at which CheA autophosphorylates. CheA$_P$ transfers its phosphoryl group to the response regulators CheY (Y) and CheB (B). CheY$_P$ subsequently binds the flagellar motor and causes the cells to change swimming direction. CheB$_P$ in conjunction with CheR (R) resets the signalling state of the MCPs, allowing the system to adapt. CheZ is a phosphatase for CheY$_P$ and is necessary for signal termination.

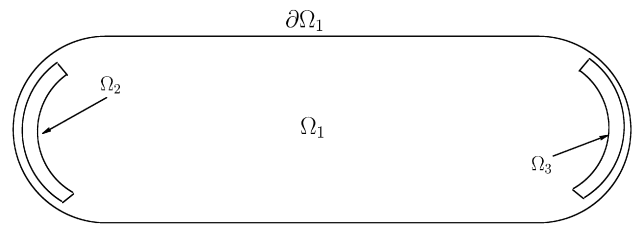

Fig. 2. A schematic representation of our two-dimensional model of an *E. coli* cell. CheA and CheZ are constrained to Ω_2 and Ω_3, whilst CheY and CheB (unphosphorylated and phosphorylated) are free to diffuse throughout all regions of the cell. The outer boundary of the cell is denoted by $\partial\Omega_1$ and the remaining cytoplasmic region by Ω_1.

and in which CheY and CheB are free to diffuse throughout all regions of the cell. Ω_1 denotes the cytoplasmic region of the cell and $\partial\Omega_1$ is the bacterial membrane. Phosphotransfer and CheZ mediated dephosphorylation of CheY$_P$ only occurs in regions Ω_2 and Ω_3, whilst autodephosphorylation of CheY$_P$ and CheB$_P$ occurs throughout all regions. Proteins can not diffuse outside the membrane of the cell. We have considered a 2-D cell here for both modelling and computational reasons. Given the symmetrical nature of the bacterium a 3-D cell is both computationally intensive to simulate and does not yield any new information. A 2-D formulation allows asymmetrical features to be considered (in future work), does not require excessive computational time and 1-D solutions (where symmetry allows, as is the case here) can be considered.

It is known that CheY forms a number of intermediary complexes with CheA and CheZ during phosphotransfer to and dephosphorylation by them, namely CheA·CheY, CheA$_P$·CheY, CheA·CheY$_P$ and CheY$_P$·CheZ, as summarised in Fig. 3.

Applying the law of mass action to the reactions shown in Fig. 3 we arrive at the following system of equations. In Ω_2 and Ω_3

$$\frac{\partial A}{\partial t} = -k_1(L)A + k_3A_PB + k_8I_2 - k_{-8}AY_P - k_9AY + k_{-9}I_3, \qquad [1]$$

$$\frac{\partial A_P}{\partial t} = k_1(L)A - k_2A_PY + k_{-2}I_1 - k_3A_PB, \qquad [2]$$

$$\frac{\partial I_1}{\partial t} = k_2A_PY - k_{-2}I_1 - k_7I_1 + k_{-7}I_2 + k_{10}(L)I_3, \qquad [3]$$

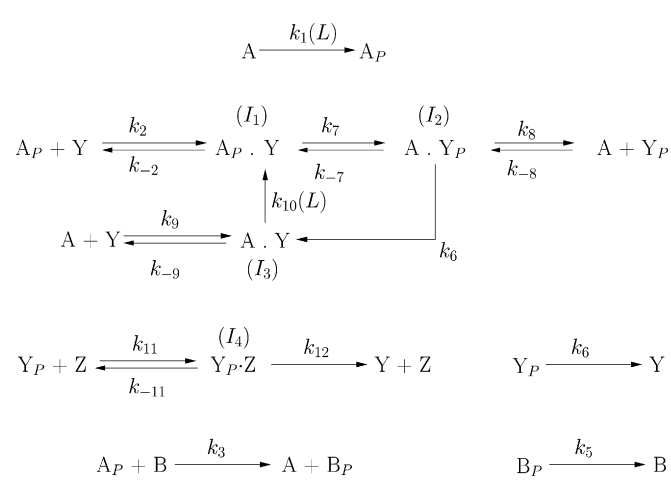

Fig. 3. The reactions considered in this model including the extended sequence of phosphotransfer reactions detailing the complexes formed in the CheY pathway. All model parameters are detailed in Table 1. We utilise the notation I_1 to represent the concentration of CheA$_P$·CheY, I_2 for CheA·CheY$_P$, I_3 for CheA·CheY and I_4 for CheY$_P$·CheZ, respectively. L is the ligand attractant concentration.

$$\frac{\partial I_2}{\partial t} = -k_6 I_2 + k_7 I_1 - k_{-7} I_2 - k_8 I_2 + k_{-8} A Y_P, \quad [4]$$

$$\frac{\partial I_3}{\partial t} = k_6 I_2 + k_9 A Y - k_{-9} I_3 - k_{10}(L) I_3, \quad [5]$$

$$\frac{\partial I_4}{\partial t} = k_{11} Y_P Z - k_{-11} I_4 - k_{12} I_4, \quad [6]$$

$$\frac{\partial Y}{\partial t} = D_Y \nabla^2 Y - k_2 A_P Y + k_{-2} I_1 - k_9 A Y + k_{-9} I_3 + k_{12} I_4 + k_6 Y_P, \quad [7]$$

$$\frac{\partial Y_P}{\partial t} = D_Y \nabla^2 Y_P + k_8 I_2 - k_{-8} A Y_P - k_{11} Y_P Z + k_{-11} I_4 - k_6 Y_P, \quad [8]$$

$$\frac{\partial Z}{\partial t} = -k_{11} Y_P Z + k_{-11} I_4 + k_{12} I_4, \quad [9]$$

$$\frac{\partial B}{\partial t} = D_B \nabla^2 B - k_3 A_P B + k_5 B_P, \quad [10]$$

$$\frac{\partial B_P}{\partial t} = D_B \nabla^2 B_P + k_3 A_P B - k_5 B_P, \quad [11]$$

and in Ω_1

$$\frac{\partial Y}{\partial t} = D_Y \nabla^2 Y + k_6 Y_P, \quad [12]$$

$$\frac{\partial Y_P}{\partial t} = D_Y \nabla^2 Y_P - k_6 Y_P, \quad [13]$$

$$\frac{\partial B}{\partial t} = D_B \nabla^2 B + k_5 B_P, \quad [14]$$

$$\frac{\partial B_P}{\partial t} = D_B \nabla^2 B_P - k_5 B_P, \quad [15]$$

where A = [CheA], A_P = [CheA$_P$], Y = [CheY], Y_P = [CheY$_P$], B = [CheB], B_P = [CheB$_P$], Z = [CheZ], I_1 = [A$_P$ Y], I_2 = [A Y$_P$], I_3 = [A Y], I_4 = [Y$_p$. Z] and L is the extracellular ligand concentration. Here we have assumed that the diffusion coefficient of unphosphorylated and phosphorylated CheYT and and CheB, respectively, are the same. The respective reaction rates and diffusion coefficients are detailed in Table 1.

The functions $k_1(L)$ and $k_{10}(L)$ are defined as

$$k_1(L) = k_1\left(1 - L^h / \left(K^h + L^h\right)\right) = k_{10}(L), \quad [16]$$

where K is a Michaelis–Menten constant and h is a Hill coefficient and we have assumed that the respective rates k_1 and k_{10} are equivalent. This simple description has been used by a number of authors as described in Albert et al. (2004) to link the extracellular concentration of an attractant ligand to the change in autophosphorylation rate of CheA. In what follows we take $K = 2.6\mu M$ and $h = 1.2$ (Sourjik and Berg, 2002b) and consider the bacterial response to an attractant of concentration $L = 10$ μM. The ligand concentration is described by

$$L = \begin{cases} 10\ \mu\text{M}, & t_0 < t < t_1, \\ 0, & \text{otherwise}, \end{cases} \quad [17]$$

where t_0 is the time at which the ligand is added and t_1 is when it is removed.

Table 1
Parameter values used in our model as obtained from the indicated sources.

Parameter	Description	Value	Reference
k_1	Rate of CheA autophosphorylation	3.75 s^{-1}	Assumed
k_2	Rate of phosphotransfer from CheA$_P$ + CheY to I_1	2.50×10^6 $(Ms)^{-1}$ [c]	Stewart (1997)
k_{-2}	Rate of I_1 to CheA$_P$ and CheY	15 s^{-1} [c]	Stewart (1997)
k_3	Rate of phosphotransfer from CheA$_P$ to CheB	1.5×10^7 $(Ms)^{-1}$	Bray website data[b]
k_5	Rate of CheB$_P$ natural dephosphorylation	0.7 s^{-1}	Stewart (1993)
k_6	Rate of CheY$_P$ natural dephosphorylation and A·Y$_p$ to A·Y	8.5×10^{-2} s^{-1}	Sourjik and Berg (2002a)
k_7	Rate of I_1 to I_2	650 s^{-1}	Stewart (1997)
k_{-7}	Rate of I_2 to I_1	50 s^{-1}	Stewart (1997)
k_8	Rate of I_2 to CheA + CheY$_P$	250 s^{-1} [d]	Li et al. (1995)
k_{-8}	Rate of CheA + CheY$_P$ to I_2	2.08×10^7 $(Ms)^{-1}$ [d]	Li et al. (1995)
k_9	Rate of CheA + CheY to I_3	7.50×10^6 $(Ms)^{-1}$	Stewart and van Bruggen (2004)
k_{-9}	Rate of I_3 to CheA + CheY	15 s^{-1}	Stewart and van Bruggen (2004)
k_{10}	Rate of I_3 to I_1	3.75 s^{-1}	Assumed equivalent to k_1
k_{11}	Rate of CheY$_P$ + CheZ to I_4	5.60×10^6 $(Ms)^{-1}$	Silversmith et al. (2008)
k_{-11}	Rate of I_4 to CheY$_P$ + CheZ	0.04 s^{-1}	Silversmith et al. (2008)
k_{12}	Rate of I_4 to CheY + CheZ	4.90 s^{-1}	Silversmith et al. (2008)
D_Y	CheY diffusion coefficient	10 μm^2 s^{-1}	Elowitz et al. (1999) Segall et al. (1985)
D_{Y_P}	CheY$_P$ diffusion coefficient	10 μm^2 s^{-1}	Segall et al. (1985) Elowitz et al. (1999)
D_B	CheB diffusion coefficient	7 μm^2 s^{-1}	Assumed[a]
D_{B_P}	CheB$_P$ diffusion coefficient	7 μm^2 s^{-1}	Assumed[a]
A_T	Total CheA concentration	7.9 μM[e]	Bray website data[b]
Y_T	Total CheY concentration	9.70 μM	Bray website data[b]
B_T	Total CheB concentration	0.28 μM	Bray website data[b]
Z_T	Total CheZ concentration	3.8 μM[e]	Bray website data[b]
L_x	Average length of a cell	3 μm	Darnton et al. (2007)
L_y	Average width of a cell	1 μm	Darnton et al. (2007)

[a] Calculated using the Einstein diffusion approximation.
[b] www.pdn.cam.ac.uk/groups/comp-cell/Rates.html.
[c] Approximated using the stated dissocation value of $K_D = 6$ μM as a guide.
[d] Calculated from a dissociation value of $K_D = 4.0$ μM.
[e] In our model setup the total size of the polar region is approximately 1/10th the volume of the cell and thus these concentrations are increased tenfold.

The initial conditions in Ω_1 are given by

$$Y(\mathbf{x},0)=Y_0,\ Y_P(\mathbf{x},0)=0,\ B(\mathbf{x},0)=B_0 \text{ and } B_P(\mathbf{x},0)=0, \quad [18]$$

and in Ω_2 and Ω_3

$$A(\mathbf{x},0)=A_0,\ A_P(\mathbf{x},0)=0,\ I_1(\mathbf{x},0)=0,\ I_2(\mathbf{x},0)=0,\ I_3(\mathbf{x},0)=0$$
$$I_4(\mathbf{x},0)=0,\ Y(\mathbf{x},0)=Y_0,\ Y_P(\mathbf{x},0)=0,\ Z(\mathbf{x},0)=Z_0,\ B(\mathbf{x},0)=B_0$$
$$\text{and } B_P(\mathbf{x},0)=0, \quad [19]$$

i.e. all proteins are initially assumed to be unphosphorylated, where A_0, Y_0 and B_0 are the initial concentrations of CheA, CheY and CheB respectively. This leads to $A_0=A_T$, $Y_0=Y_T$ and $B_0=B_T$, where A_T, Y_T and B_T represent the total concentration (unphosphorylated and phosphorylated) of CheA, CheY and CheB, respectively. Furthermore $Z_0=Z_T$. Here $\mathbf{x}=(x,y)$.

The boundary conditions on $\partial\Omega_1$ are defined by

$$\hat{n}\cdot\nabla Y(\mathbf{x},t) = 0, \quad \hat{n}\cdot\nabla Y_P(\mathbf{x},t) = 0,$$
$$\hat{n}\cdot\nabla B(\mathbf{x},t) = 0 \quad \text{and} \quad \hat{n}\cdot\nabla B_P(\mathbf{x},t) = 0. \quad [20]$$

where $\hat{n}$ is a unit vector normal to the surface of the cell. The flux of Y, Y_P, B and B_P is taken to be continuous between each of the three regions; Ω_1, Ω_2 and Ω_3.

The governing equations (1)–(15) with the respective boundary and initial conditions were solved computationally using the finite element solver COMSOL (COMSOL, Stockholm). The model was allowed to reach a steady-state before the attractant stimulus was applied as defined by equation (17). Given the symmetry of our model bacterium (see Fig. 2) around the central axis, solutions were only considered in one spatial dimension along the length of the cell (from pole-to-pole).

3. Results and discussion

3.1. Spatial distribution of CheY in wild-type cells

We have used the model described in Section 2 to predict the spatial distribution of CheY in wild-type cells. Fig. 4(a) shows the distribution of CheY in all of its forms ($CheY_{Total}$), i.e. CheY, $CheY_P$, CheA·CheY, CheA·$CheY_P$, $CheA_P$·CheY and $CheY_P$·CheZ. Fig. 4(b) shows the distribution of phosphorylated CheY in all of its forms ($CheY_{PAll}$) i.e. $CheY_P$, CheA·$CheY_P$ and $CheY_P$·CheZ, while Fig. 4(c) shows the distribution of unphosphorylated CheY in all of its forms ($CheY_{All}$) i.e. CheY, CheA·CheY and $CheA_P$·CheY.

Interestingly, the distribution of $CheY_{Total}$ does not change significantly between high and low kinase activity (pre- and post-stimulus), respectively (Fig. 4). However, the levels of $CheY_{All}$ and $CheY_{PAll}$ change considerably (Fig. 4(b) and (c)), with high kinase activity giving higher levels of $CheY_{PAll}$ and lower levels of $CheY_{All}$ throughout the cell. CheA and CheZ have been confined to the polar regions, therefore all of the complexes of CheY are also confined to the polar regions. This means that any $CheY_{PAll}$ and $CheY_{All}$ outside the polar region (more than 0.1 μm along the cell) reflect the free concentrations of $CheY_P$ and CheY respectively.

Previous studies have concluded that the localization of the phosphatase, CheZ, to the polar cluster, minimizes the formation of spatial gradients of $CheY_P$ along the length of the cell (Vaknin and Berg, 2004; Lipkow et al., 2005). In line with these studies, our model predicts that outside the polar regions there is a uniform concentration of free $CheY_P$ along the length of the cell. Since the flagella are distributed randomly along the length of the cell, this implies that each motor will experience an equivalent $CheY_P$ concentration regardless of its distance from the polar cluster.

The switching behaviour of the flagellar motor at different concentrations of $CheY_P$ has been experimentally studied (Cluzel

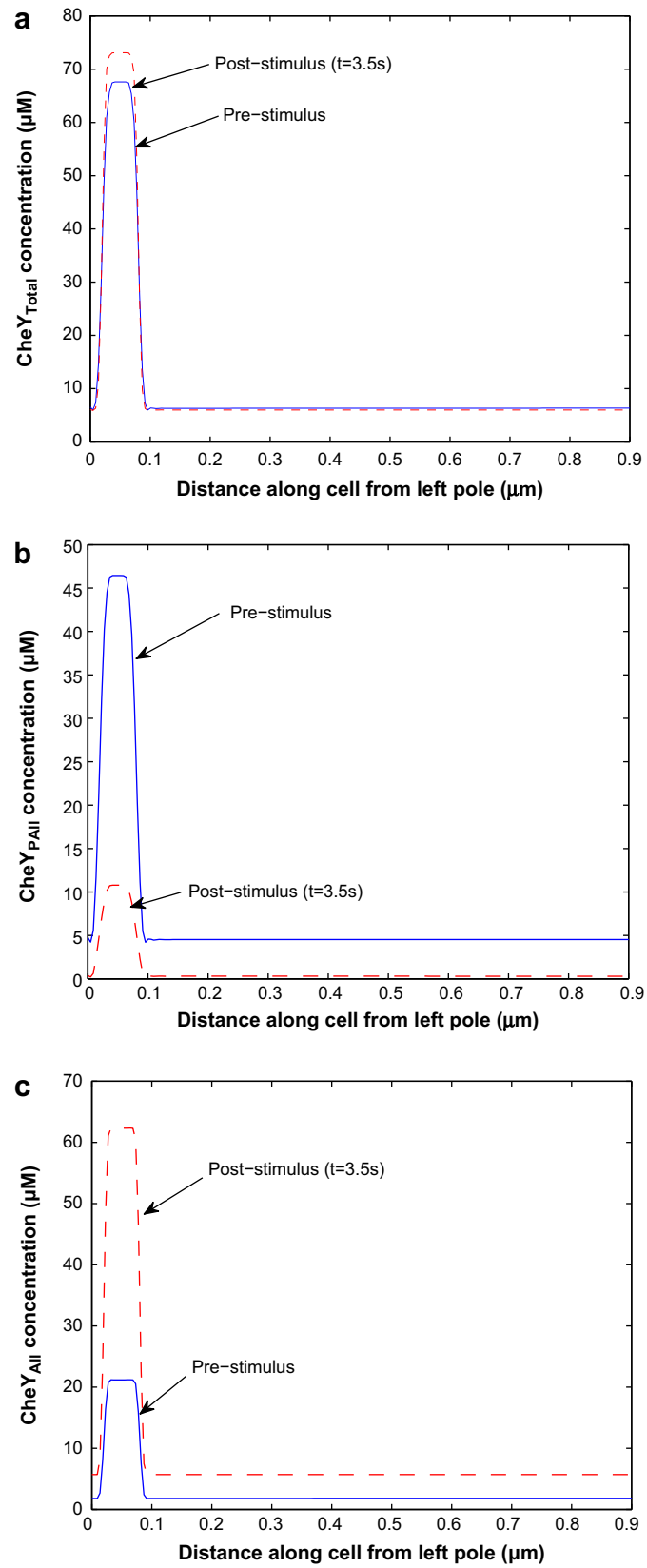

Fig. 4. The spatial variation in: (a) $CheY_{Total}$ (CheY + $CheY_P$ + $CheA_P$·CheY + CheA·CheY + CheA·$CheY_P$ + $CheY_P$·CheZ); (b) $CheY_{PAll}$ concentration ($CheY_P$ + CheA·$CheY_P$ + $CheY_P$·CheZ); and (c) $CheY_{All}$ (CheY + CheA·CheY + $CheA_P$·CheY) along the length of the cell when an attractant gradient (L = 10 μM) is detected by a wild-type cell.

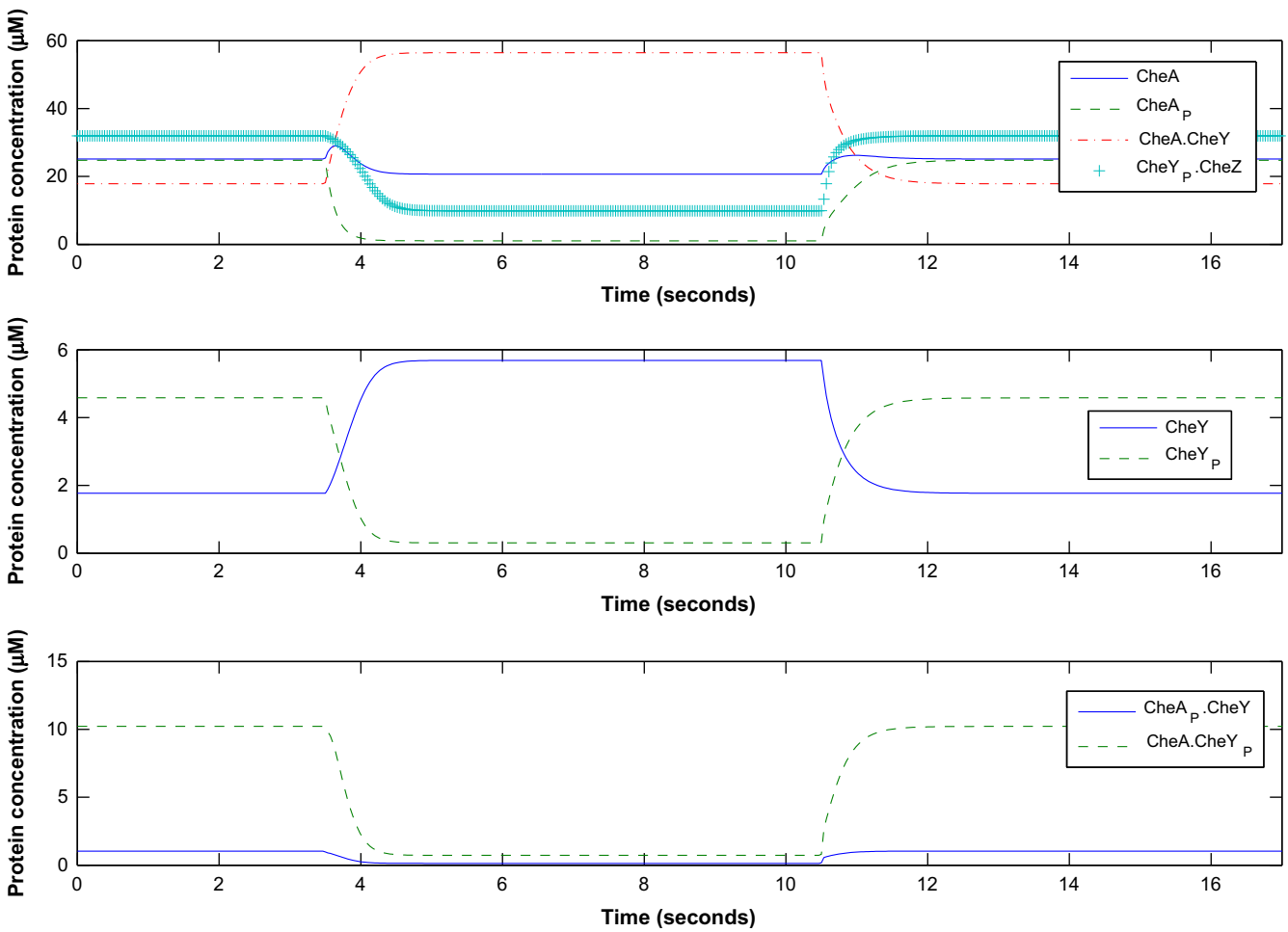

Fig. 5. The dynamical variation in: (upper) CheA, CheA$_P$, CheA·CheY and CheY$_P$·CheZ; (middle) CheY and CheY$_P$; and (lower) CheA$_P$·CheY and CheA·CheY$_P$ at the polar receptor clusters, before, during and after an attractant ($L = 10$ μM) has been detected by a wild-type cell. The attractant is added at $t = 3.5$ s and removed at $t = 10.5$ s.

et al., 2000). The motor rotates almost exclusively clockwise at CheY$_P$ concentrations exceeding 4 μM, while rotating almost exclusively counter-clockwise at CheY$_P$ concentration below 2 μM. Our model predicts that upon switching from high kinase activity to low kinase activity, the level of free CheY$_P$ in the cytoplasm falls from 4.6 μM to 0.3 μM indicating that a switch from clockwise to counter-clockwise rotation would occur.

3.2. Dynamic variation of CheY containing complexes in a wild-type cell

We simulated the response of cells to the addition and subsequent removal of 10 μM attractant as shown in Fig. 5. Prior to the addition and after the removal of attractant, the kinase activity of CheA was high, while in the presence of attractant, kinase activity was low. When CheA kinase activity was high, the majority of CheA$_{Total}$ was not complexed with CheY. In contrast, when kinase activity was low the majority of CheA$_{Total}$ was in the form of a CheA·CheY complex. Interestingly, approximately one-third of CheA$_{Total}$ was present as unphosphorylated and uncomplexed CheA, regardless of whether kinase activity was high or low (Fig. 5). The increased formation of the CheA·CheY complex prevents unphosphorylated uncomplexed CheA accumulating even when kinase activity is reduced. Upon addition of the attractant, CheY$_P$ takes 0.45 s to drop below the 2 μM tumble threshold (Cluzel et al., 2000). The same timescale is observed for CheY$_P$ levels to increase on removal of the attractant.

3.3. Effect of CheZ expression levels on the spatial distribution of CheY

Due to the ability of our model to predict the spatial localization of CheY$_{Total}$ in bacterial cells, we attempted to simulate the experimental data of Vaknin and Berg (Vaknin and Berg, 2004), who observed a difference in CheY localization upon attractant stimulation of cells either over- or under-expressing CheZ. In their experiments, high CheZ expression was induced with 0.01% arabinose from plasmid pVS54; in Kentner and Sourjik this level of induction was reported to give a total CheZ concentration of 11.7 μM (Kentner and Sourjik, 2009), which is ~3 fold higher than the wild-type level of 3.8 μM. Low levels of expression refer to arabinose concentrations of less than 0.0003%. In cells expressing low levels of CheZ, the association of CheY with the polar cluster increased in attractant. In contrast, in cells expressing high levels of CheZ, the association of CheY with the cluster decreased in attractant.

We simulated the addition of attractant to cells over-expressing ($Z_T = 12$ μM) or under-expressing ($Z_T = 0.1$ μM) CheZ and examined the localization of CheY$_{Total}$ in these cells. Consistent with the results of Vaknin and Berg (Vaknin and Berg, 2004), our model predicts that when CheZ is under-expressed then the polar localization of CheY$_{Total}$ is highest in attractant (low kinase activity), while when CheZ is over-expressed, the polar localization of CheY$_{Total}$ is highest without attractant (high kinase activity) (Fig. 6).

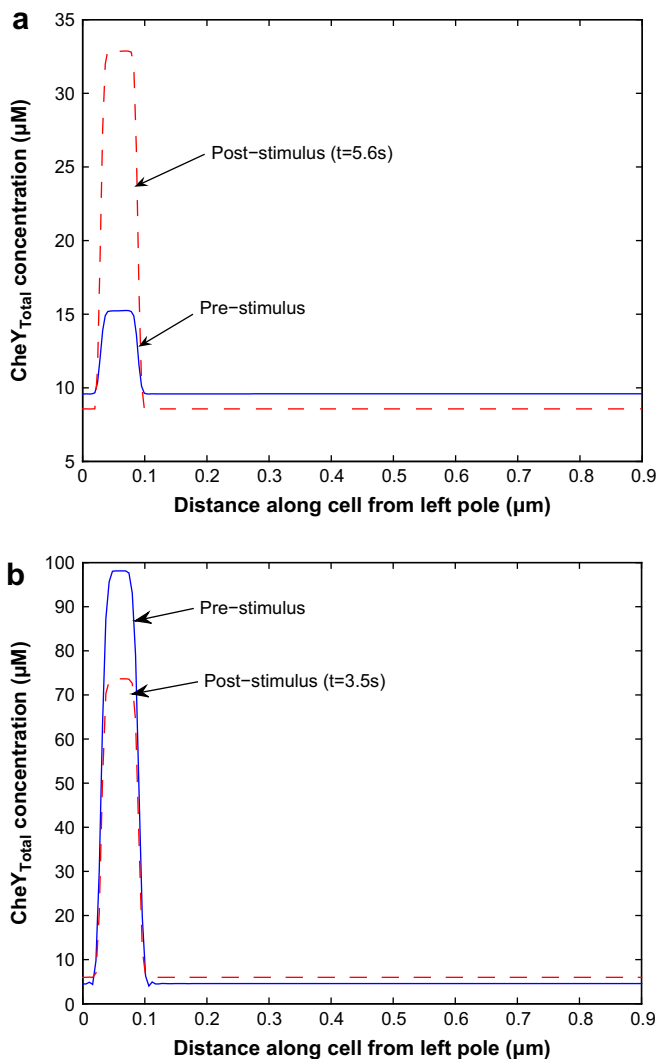

Fig. 6. The variation in $CheY_{Total}$ when CheZ is: (a) under-expressed ($Z_T = 0.1$ μM); and (b) over-expressed ($Z_T = 12$ μM) and an attractant gradient ($L = 10$ μM) is detected. Results agree with those found experimentally by Vaknin and Berg (2004). The time for each post-stimulus response differs due to the time taken for the system to reach its post-stimulus steady-state.

3.4. Analysis of CheY complex formation

Given the ability of our model to reproduce the CheY localization data of Vaknin and Berg (Vaknin and Berg, 2004), we proceeded to examine the relative fraction of $CheY_{Total}$ in each complex during a chemotactic response. In wild-type cells, approximately 40% of CheY is bound in protein-complexes at the cell poles rather than freely diffusing in the cytoplasm (Table 2). Interestingly, in a wild-type cell this fraction does not change dramatically pre- or post-stimulus. This means that there is no dramatic change in the distribution of $CheY_{Total}$, whether the kinase activity of CheA is high or low. However, when kinase activity is high most of the complexed CheY exists as $CheY_P$·CheZ, whereas when kinase activity is low most is in a CheA·CheY complex.

In contrast with wild-type cells, cells over-expressing CheZ show a different pattern of $CheY_{Total}$ distribution pre- and post-stimulus (Table 2). While the post-stimulus localization of $CheY_{Total}$ was similar to that of wild-type cells, with ~40% being bound in complexes at the cell pole, pre-stimulus more than 50% of $CheY_{Total}$ was associated with polar complexes. The over-expression of CheZ increases the polar localization of $CheY_{Total}$ under conditions of high kinase activity for two reasons. Firstly, it allows more $CheY_P$·CheZ complexes to form, and secondly its phosphatase activity increases the amount of free CheY and hence the amount of CheA·CheY complex.

In cells in which CheZ is under-expressed, levels of $CheY_P$ are high both pre- and post-stimulus with relatively few CheY complexes (Table 2). This is unsurprising given the limited amount of CheZ available to dephosphorylate $CheY_P$. The most abundant complex is the CheA·$CheY_P$ complex, whose formation is favoured by low CheA kinase activity post-stimulus. This results in increased polar localization of $CheY_{Total}$ post-stimulus.

4. Conclusions

We have developed a spatiotemporal mathematical model of the phosphosignalling reactions of *E. coli* chemotaxis that includes the formation of the following CheY containing complexes: CheA·CheY, $CheA_P$·CheY, CheA·$CheY_P$ and $CheY_P$·CheZ. Consistent with experimental observations, we have restricted the localization of CheA and CheZ to a region at the poles of the cell, whilst allowing uncomplexed CheY and $CheY_P$ to diffuse freely throughout the cell. In response to the addition and removal of 10 μM attractant, our model predicts that the concentration of free $CheY_P$ in the cytoplasm changes from 4.6 μM to 0.3 μM, neatly crossing the range of 4–2 μM, shown by Cluzel et al. (2000) to be required to generate a chemotactic response. In addition, the model reproduces the experimental observations of Vaknin and Berg (2004), showing differences in CheY localization during a chemotactic response in cells over- or under-expressing CheZ. Importantly the model also shows that in wild-type cells, 40% of $CheY_{Total}$ is bound in protein complexes at the poles and hence not available to bind FliM and cause switching. This demonstrates the importance of considering protein localization and clustering when modelling biological pathways.

Table 2
Model results detailing CheY in its free and complex forms (unphosphorylated and phosphorylated) expressed as a percentage of $CheY_{Total}$, pre- and post-stimulus. Results are shown for wild-type cells and cells under- and over-expressing CheZ.

	CheY free	$CheY_P$ free	CheA·CheY	CheA·$CheY_P$	$CheA_P$·CheY	$CheY_P$·CheZ
Wild-type ($Z_T = 3.8$ μM)						
Pre-stimulus	18.56	46.97	10.20	5.83	0.59	17.91
Post-stimulus	58.62	3.15	32.22	0.41	0.07	5.51
Low CheZ ($Z_T = 0.1$ μM)						
Pre-stimulus	1.74	95.23	0.16	2.17	0.18	0.51
Post-stimulus	4.7	81.98	2.85	9.22	0.73	0.51
High CheZ ($Z_T = 12$ μM)						
Pre-stimulus	40.64	6.55	22.77	1.33	0.32	28.39
Post-stimulus	60.81	0.81	32.56	0.18	0.06	5.57

Acknowledgements

PKM was partially supported by a Royal Society Wolfson Merit Award.

References

Albert, R., Chiu, Y., Othmer, H., 2004. Dynamic receptor team formation can explain the high signal transduction gain in *Escherichia coli*. Biophys. J. 86, 2650–2659.

Bray, D., Levin, M., Morton-Firth, C., 1998. Receptor clustering as a cellular mechanism to control sensitivity. Nature 393 (7), 85–88.

Bray-Group, 2009. Computational cell biology Experimental data (1998). http://www.pdn.cam.ac.uk/groups/comp-cell/Rates.html#references (Last accessed 01.06.09).

Cluzel, P., Surette, M., Leibler, S., 2000. An ultrasensitive bacterial motor revealed by monitoring signaling proteins in single cells. Science 287, 1652–1654.

Darnton, N., Turner, L., Rojevsky, S., Berg, H., 2007. On torque and tumbling in swimming *Escherichia coli*. J. Bacteriol. 189 (5), 1756–1764.

Elowitz, M., Surette, M., Wolf, P., Stock, J., Leibler, S., 1999. Protein mobility in the cytoplasm of Escherichia coli. J. Bacteriol. 181 (1), 197–203.

Kentner, D., Sourjik, V., 2009. Dynamic map of protein interactions in the *Escherichia coli* chemotaxis pathway. Mol. Syst. Biol. 5, 238. Epub.

Li, J., Swanson, R., Simon, M., Weis, R., 1995. The response regulators cheb and chey exhibit competitive binding to kinase chea. Biochemistry 34, 14626–14636.

Li, M., Hazelbauer, G., 2004. Cellular stoichiometry of the components of the chemotaxis signalling complex. J. Bacteriol. 186, 3687–3694.

Lipkow, K., Andrews, S., Bray, D., 2005. Simulated diffusion of phosphorylated CheY through the cytoplasm of *Escherichia coli*. J. Bacteriol. 187 (1), 45–53.

Maddock, J., Shapiro, L., 1993. Polar location of the chemoreceptor complex in the *Escherichia coli* cell. Science 259 (9), 1717–1723.

Segall, J., Ishihara, A., Berg, H., 1985. Chemotactic signalling in filamentous cells of Escherichia coli. J. Bacteriol. 161 (1), 51–59.

Silversmith, R., Levin, M., Schilling, E., Bourret, R., 2008. Kinetic characterization of catalysis by the chemotaxis phosphatase chez. J. Biol. Chem. 283, 756–765.

Sourjik, V., Berg, H., 2000. Localization of components of the chemotaxis machinery of *Escherichia coli* using fluorescent protein fusions. Mol. Microbiol. 37 (4), 740–751.

Sourjik, V., Berg, H., 2002a. Binding of the *Escherichia coli* response regulator CheY to its target measured *in vivo* by fluorescence resonance energy transfer. Proc. Natl. Acad. Sci. U.S.A. 99, 12669–12674.

Sourjik, V., Berg, H., 2002b. Receptor sensitivity in bacterial chemotaxis. Proc. Natl. Acad. Sci. U.S.A. 99 (1), 123–127.

Stewart, R., 1993. Activating and inhibitory mutations in the regulatory domain of CheB, the methylesterase in bacterial chemotaxis. J. Biol. Chem. 268 (3), 1921–1930.

Stewart, R., 1997. Conference presentation. BLAST.

Stewart, R., van Bruggen, R., 2004. Rapid phosphotransfer to CheY from a CheA protein lacking the CheY-binding domain. Biochemistry – US 43 (27), 8766–8777.

Vaknin, A., Berg, H., 2004. Single-cell FRET imaging of phosphatase activity in the *Escherichia coli* chemotaxis system. Proc. Natl. Acad. Sci. U.S.A. 101 (49), 17072–17077.

Wadhams, G., Armitage, J., 2004. Making sense of it all: bacterial chemotaxis. Nat. Rev. Mol. Cell Biol. 5 (12), 1024–1037.